RSC Advances

PAPER

View Article Online
View Journal | View Issue

Cite this: *RSC Adv.*, 2023, **13**, 11720

H_2O_2 activated moxa ash *via* ball milling for ultrafast removal of mitoxantrone†

Wanqian Cai,[a] Chongbiao Zhang,[a] Yourong Wu,[a] Wei Wang,[a] Mei Lin,*[b] Tengfei Lin,[a] Cong Lin,[a] Min Gao,[a] Chunlin Zhao[a] and Xiao Wu*[a]

As emerging contaminants, antineoplastic drugs are widely used, but their residues in water may cause long-term genotoxicity to aquatic organisms and human beings. Here, waste moxa ash was selected as biomass raw material and modified by ball milling to obtain carbon-based materials with excellent adsorption performance, which were used to remove the antineoplastic drug mitoxantrone (MTX) from water. The experimental results indicate that moxa ash modified by ball milling in hydrogen peroxide exhibits ultrafast removal of MTX (the removal efficiency reaches 97.66% in 1 min and 99.72% in 30 min). The pseudo-second-order kinetics and Freundlich isotherm models accurately describe the MTX adsorption process, and the mechanism of adsorption probably involves pore filling, hydrogen bond, $\pi-\pi$ interaction and electrostatic attraction. Not only that, moxa ash also has the ability to remove dyes such as malachite green (97.81%) and methylene blue (99.97%). In this study, a simple and environmentally friendly process was used to convert waste moxa ash into an effective MTX adsorbent, providing a feasible solution for controlling MTX pollution and identifying a circular and economic way to reuse the waste.

Received 13th February 2023
Accepted 11th April 2023

DOI: 10.1039/d3ra00988b

rsc.li/rsc-advances

1. Introduction

Currently, the intake of antineoplastic drugs is gradually increasing, while most of them are not naturally degradable and conventional wastewater treatment methods are not sufficient to get rid of them.[1] This fact leads to the persistence of drugs in water sources, including drinking water, surface water and groundwater, posing a serious threat to both human health and environmental sustainability.[2,3] Mitoxantrone (MTX) is a synthetic anthraquinone antitumor drug (Fig. S1†), and its remarkable efficacy in the treatment of various malignancies has led to widespread production and use at present.[4] However, approximately 31–36% of MTX is not metabolized and is directly excreted into the aquatic environment, which can damage aquatic resources and endanger human health.[5] Therefore, it is urgent to effectively remove MTX from wastewater.

Various types of water purification technologies, such as membrane filtration,[6–8] adsorption,[9] biological treatment[10] and advanced oxidation[11] have been developed. Among them, adsorption-based technologies show prominent advantages of being inexpensive, efficient and easy to operate.[12] Although some novel adsorbents such as metal–organic frameworks and layered double hydroxides exhibit remarkable adsorption capacity,[13,14] their large-scale production is greatly hampered by existing technological limitations such as complex synthesis processes, the use of toxic organic chemicals and high energy consumption. In contrast, carbon-based adsorbents such as activated carbon and biochar,[15,16] which are abundant in source, easy to prepare and low in cost, have been widely used for the removal of pollutants from water. Recently, the use of agricultural and industrial wastes generated by human activities to produce economic and environmental friendly carbon-based adsorbents has attracted widespread attention.[17] For instance, raw sugarcane bagasse was employed to remove ciprofloxacin, exhibiting an initial removal ratio of 65% and a maximal adsorption capacity of 13.6 mg g^{-1}.[18] Tetracycline (50 mg L^{-1}) antibiotics could be adsorbed by spent coffee grounds, and shaking for 2 h resulted in clearance rates of 97.2%.[19]

In recent years, moxibustion has been used more frequently as the global healthcare burden has increased, including rising healthcare costs and the continued increase in chronic non-communicable diseases.[20] Additionally, it also plays a crucial part in the present COVID-19 intervention.[21] The raw material used in moxibustion is moxa, which is made from dried mugwort leaves that have been crushed and sifted through several rounds. During the use of moxibustion, moxa begins to burn and produces moxa ash, which is often discarded as garbage. In our current research, we find moxa ash is a highly promising adsorbent material that can be further modified to prepare excellent green adsorbents for controlling contamination of pharmaceuticals in wastewater.

[a]*College of Materials Science and Engineering, Fuzhou University, Fuzhou, 350108, China. E-mail: wuxiao@fzu.edu.cn*

[b]*College of Environment and Resource Science, Fujian Normal University, Fuzhou 350007, Fujian Province, China. E-mail: linmei706@fjnu.edu.cn*

† Electronic supplementary information (ESI) available. See DOI: https://doi.org/10.1039/d3ra00988b

Most raw biomass materials have a low adsorption capacity and selection for pollutants, which can be overcome by surface modification to enhance adsorption performance.[22] As a simple and environmentally friendly method, ball milling has received a lot of attention.[23] For example, pharmaceuticals may be effectively removed using biochar made from ball-milled hickory wood chips, having maximum adsorption capacities for sulfapyridine of 57.9 mg g^{-1} and sulfamethoxazole of 100.3 mg g^{-1}.[24] The greatest amount of fluconazole that could be absorbed by ball-milled magnetic biochar was close to 15.90 mg g^{-1}, which was around five times more than what could be absorbed by pristine magnetic biochar.[25] Ball milling in atmospheres or combination with other chemicals may influence the surface functional groups of adsorbent, thus altering its ability to adsorb different pollutants.[26] For instance, ball-milled biochar was modified with hydrogen peroxide (H_2O_2) and ammonia hydroxide ($NH_3 \cdot H_2O$), effectively changing the morphological characteristics and improving its adsorption capacity for aromatic volatile organic chemicals.[27] However, using H_2O_2 as a modifier in combination with ball milling for physical-chemical modification is still at a preliminary stage, especially in the field of pharmaceuticals removal.

Here, the adsorbents with excellent adsorption performance were prepared by using H_2O_2 as a chemical modifier combined with ball milling method to modify moxa ash. The as-prepared moxa ash were used to remove MTX from water. The goals of this study were to (1) compare the physical and chemical characteristics of moxa ash (MA), ball-milled MA (BMMA), ball-milled MA with H_2O (BMMA-H_2O) and ball-milled MA with H_2O_2 (BMMA-H_2O_2) obtained under different conditions, and (2) look into the MTX in water adsorption efficiency and associated mechanism.

2. Materials and methods

2.1 Materials

Chemical solutions were created using deionized (DI) water (18.2 MΩ). Mitoxantrone hydrochloride (≥97%), 30% H_2O_2, hydrochloric acid, and sodium hydroxide were obtained from Aladdin Chemistry Co., Ltd. (Shanghai, China). NaCl, Na_2CO_3, Na_2SO_4, $NaNO_3$ and humic acid (HA) were purchased from Sinopharm Chemical Reagent Co., Ltd. All reagents used above are analytically pure. Moxa was purchased from Jinan Ou Mai Medical Instrument Co., Ltd.

Moxa was ignited in the air for 5 min until the combustion was completed to obtain moxa ash (MA), and then passed through 100 meshes and rinsed repeatedly with DI water to achieve a constant pH value. In a 500 mL agate jar, 100 g of 3 mm, 5 mm, and 10 mm diameter agate balls were combined with 1 g of MA in a mass ratio of 3 : 5 : 2, with or without addition of H_2O or H_2O_2. The jar was then sealed and put into a planetary ball mill that was rotated in a different direction every 6 h while being driven at 300 rpm for 12 h.[28] The resulting samples were labelled as BMMA, BMMA-H_2O, and BMMA-H_2O_2. Fig. 1 shows a schematic process for the production and modification of moxa ash and the difference in their ability to remove MTX.

2.2 Batch sorption

To examine the adsorption capabilities of samples obtained under various ball milling circumstances, batch sorption tests were conducted. A light-proof centrifuge tube of 50 mL was filled with 25 mL of a 20 mg L^{-1} MTX solution and approximately 12.5 mg of adsorbent (0.5 g L^{-1}) to complete the dosage. Using a mechanical shaker, the mixtures were shaken continuously at a velocity of 250 rpm for 6 h at 25 °C. The samples were then filtered using a nylon membrane filter with 0.22 μm pore size. At a wavelength of 609 nm, a UV-vis spectrophotometer (UV-6000, Metash, China) was used to detect the concentrations of MTX in the aqueous phase. The capacity and removal efficiency of MTX were determined using eqn (1) and (2), respectively.

$$q_e = \frac{(C_0 - C_e)}{m} V \quad (1)$$

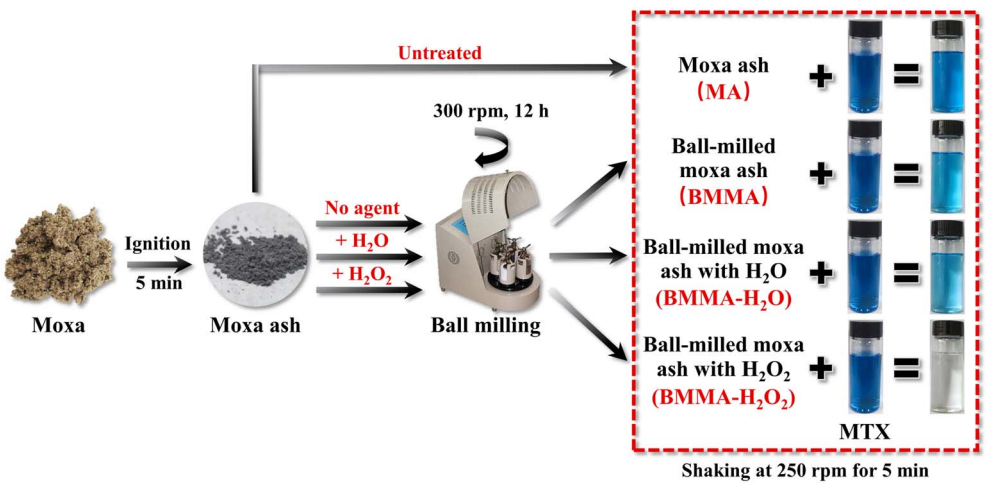

Fig. 1 A schematic representation of the manufacturing pathway of moxa ash and adsorption process before and after modification.

$$R\ (\%) = \frac{C_0 - C_e}{C_e} \times 100\% \quad (2)$$

where C_0 and C_e (mg L^{-1}) are the initial and equilibrium concentration of MTX after adsorption, respectively, V (L) and m (g) represent the volume of MTX solution and the mass of moxa ash.

To assess the adsorption kinetics, 25 mL of a 20 mg L^{-1} MTX solution and 12.5 mg of an adsorbent were added to the shaker (*i.e.*, 5, 10, 15, 20, 30, 60, 90, 120, 180, 240, 300 and 360 min). In order to create the isotherms, 25 mL of MTX was combined for 6 h with 12.5 mg of the adsorbent at beginning concentrations ranging from 10 to 200 mg L^{-1}. Subsequently, the removal efficiencies of the adsorbent for MTX were calculated at different initial concentrations of adsorbent doses (0.05 to 1.0 g L^{-1}). Using the aforementioned experimental settings, the influence of pH value on removal efficiency for the adsorbent was evaluated, and the pH of the mixture was changed from 2 to 12 by adding 0.1 M of either HCl or NaOH. The effect of external factors on the sorption selectivity of BMMA-H_2O_2 was explored by adding different concentrations (5, 10 and 20 mg L^{-1}) of HA and different species of competing anions (Cl^-, CO_3^{2-}, SO_4^{2-} and NO_3^-) at concentrations of 10 and 100 mmol L^{-1}. Finally, the removal efficiency of MTX by BMMA-H_2O_2 in real lake water was investigated. All the reported experimental data are averages obtained after three replications.

2.3 Regeneration experiments

In this study, NaOH was used to regenerate BMMA-H_2O_2. The used adsorbent was sonicated in 0.1 M NaOH solution for 15 min, repeated twice, and then washed with DI water to neutral and dried. The above experiments were repeated to test the regeneration performance of the adsorbent.

2.4 Characterization methods

MA, BMMA, BMMA-H_2O, and BMMA-H_2O_2 had their specific surface area and pore size distribution measured using a surface analyzer (BET, 2460, Micromeritics Instrument Co., USA). Scanning electron microscopy (SEM, Supra 55 Sapphire, Carl Zeiss, Germany) was used to study their structure and surface morphology. The change of groups in the treated samples was determined using a Fourier transform infrared spectrometer (FTIR, Nicolet 5700, Thermo Fisher Nicolet, USA). X-ray photoelectron spectroscopy (XPS, K-Alpha+, Thermo Fisher, USA) was measured the changes of BMMA-H_2O_2 surface elements before and after the adsorption of MTX. Using a spectrometer (Raman, DXR2xi, Thermo Fisher Scientific, USA) with an excitation wavelength of 532 nm, the Raman spectra were obtained. A zeta sizer (Nano ZS90, Malvern, UK) was used to calculate zeta potential.

3. Results and discussion

3.1 Characterization

Fig. 2a displays the SEM images of the virgin moxa ash, and the sample clearly shows a curled tree bark shape. After ball milling, the shape is broken into irregular particles (Fig. 2b–d). Obviously, the particle agglomeration of BMMA-H_2O obtained from wet ball milling is reduced and the average particle size is smaller than that of BMMA. Furthermore, the fine particles of

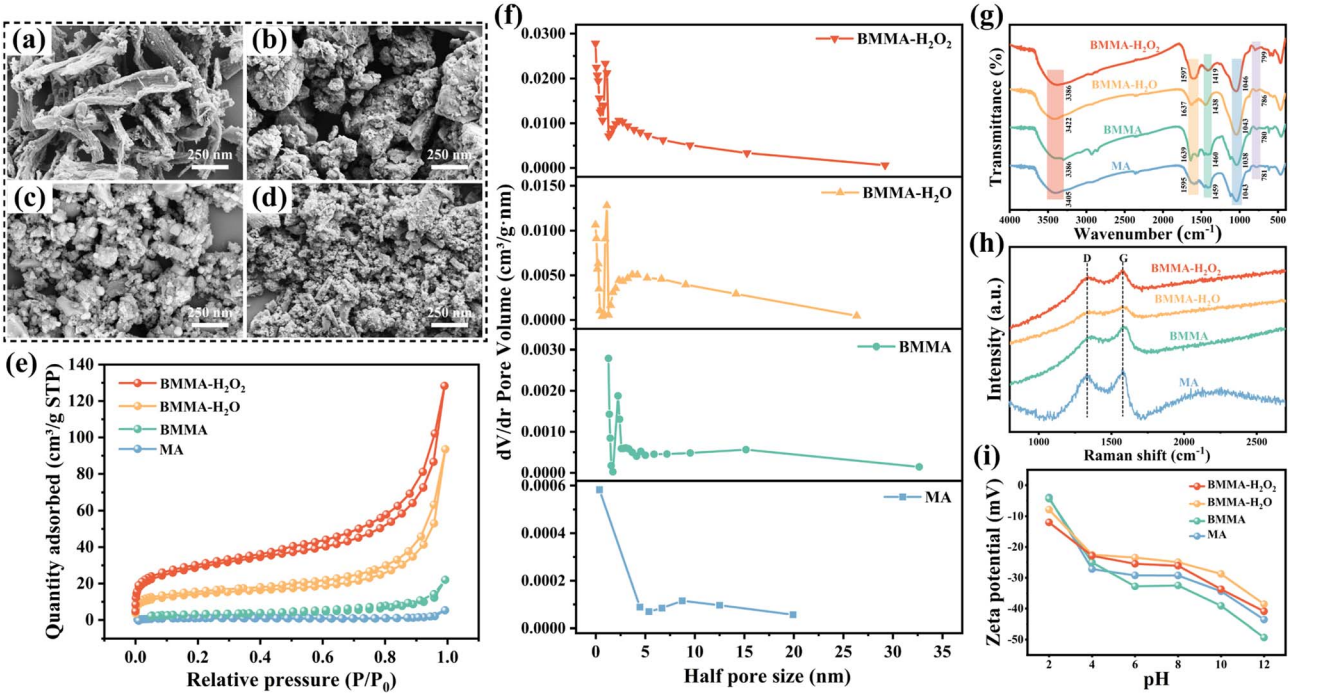

Fig. 2 SEM images of (a) MA, (b) BMMA, (c) BMMA-H_2O, (d) BMMA-H_2O_2. (e) Nitrogen adsorption–desorption isotherms, (f) pore size distribution, (g) FTIR spectra, (h) Raman spectra and (i) zeta potential.

BMMA-H_2O_2 are more uniform dispersion and regular in morphology, most of them appear rounded, probably due to H_2O_2 corrosion.[27] Uniformly dispersed particles can improve the adsorption efficiency of the adsorbent because they can provide more active sites and facilitate the interaction between the adsorbent and the pollutant molecules in the water.

The nitrogen adsorption–desorption isotherms shown in Fig. 2e are all classified by the International Union of Pure and Applied Chemistry as a combination of type I and type IV with hysteresis loops, showing that the pore architectures include both micropores and mesopores.[29] The pore diameter distribution in Fig. 2f can also be used to demonstrate the same conclusions. The specific surface area (SSA), pore volume (PV), and pore size of the samples were evaluated in order to further study the adsorption performance of the produced materials. The results are given in Table S1.† The average pore size of moxa ash become smaller after ball milling, resulting in an increase in PV and SSA values. And this variation is more evident for BMMA-H_2O and BMMA-H_2O_2. Compared to MA, the average pore size of BMMA-H_2O_2 reduces from 32.62 to 10.26 nm, while the SSA value increases from 2.89 to 96.46 $m^2\ g^{-1}$. Due to the more homogeneous fine particles created during the ball milling process, the samples that have been subjected to ball milling have greater exterior and interior surface areas. And compared to dry ball milling, the inclusion of liquid medium yields smaller, more scattered particles and more varied functional groups.[30] Besides, H_2O_2 can act as a modifier and help to further open up the closed pores of the material during the ball milling process.

The moxa ash before and after modification is alkaline (pH = 10.1) and the pH value of BMMA, BMMA-H_2O and BMMA-H_2O_2 reduces to 9.7, 9.5 and 9.3, respectively (Table S1†). Ball milling has been shown to significantly improve oxygen-containing functional groups in carbon-based materials, such as carboxyl and hydroxyl groups, which represent a source of acidity on the material surface to reduce the pH value.[31,32] FTIR spectra (Fig. 2g) corroborated the alterations in the surface functional groups of moxa ash that occurred during ball milling. All samples show four main vibrational adsorption bands in the ranges of 3386–3422 cm^{-1} (O–H), 1595–1639 cm^{-1} (aromatic C=C/C=O), 1438–1460 cm^{-1} (C–H), 1038–1070 cm^{-1} (C–O) and 780–799 cm^{-1} (aromatic C–H).[33] The strength of O–H and C–O bonds increases during ball milling, especially for BMMA-H_2O_2 where abundant hydroxyl groups are introduced.

Raman spectroscopy is used to detect defects in moxa ash and the intensity ratio between the D and G bands (I_D/I_G) is used to assess the severity of the defects. The I_D/I_G values for MA, BMMA, BMMA-H_2O and BMMA-H_2O_2 are determined to be 0.875, 0.932, 0.966, and 0.970, respectively, as depicted in Fig. 2h, indicating that the defect degree of moxa ash increases through sacrificing the degree of graphitization after ball milling.[34] The zeta potential of moxa ash shows a similar declining trend with pH value for the four samples (Fig. 2i). The moxa ash preparation is a good option for the electrostatic adsorption of pollutants with positive functional groups because the surface charge of the moxa ash is consistently negative across the whole pH range of 2 to 12.

3.2 Adsorption performance

In Fig. 3a, the removal efficiency of MTX by MA, BMMA, BMMA-H_2O, and BMMA-H_2O_2 are contrasted. The adsorption equilibrium has been attained after 5 h and the removal efficiency of MTX by MA has reached 95.7%. After modification by dry/wet ball milling, the removal efficiency of MTX by BMMA, BMMA-

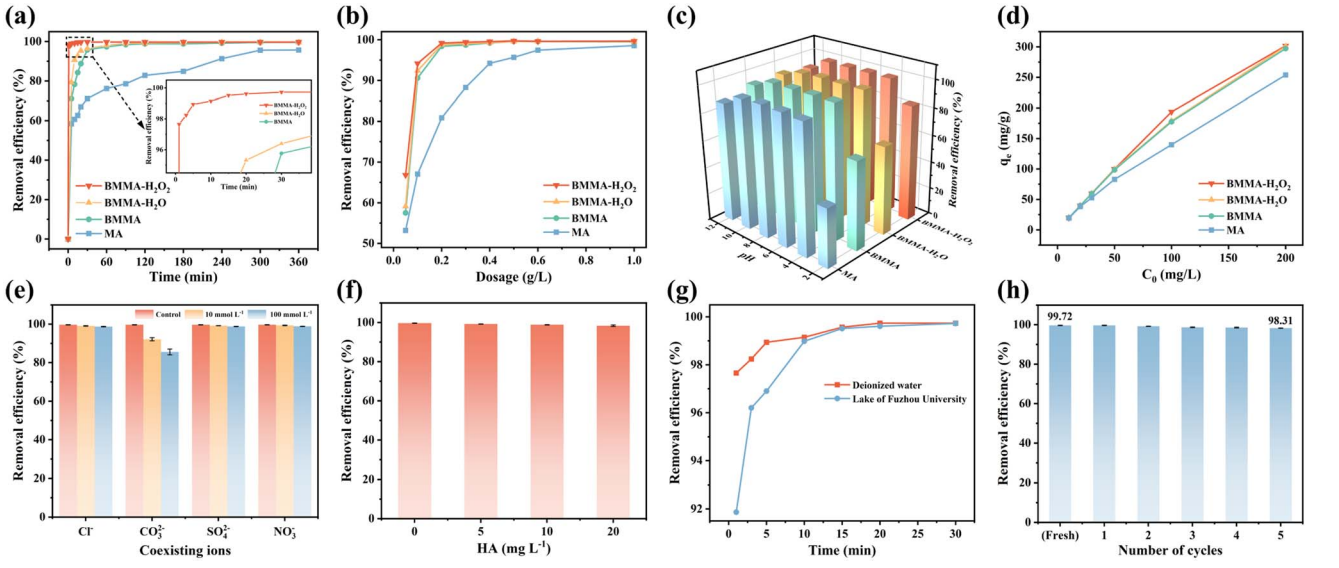

Fig. 3 The effect of (a) time, (b) absorbent dose and (c) pH on the removal efficiency of MTX by MA, BMMA, BMMA-H_2O and BMMA-H_2O_2. (d) Adsorption capacity under different initial concentrations of MTX. Effect of coexisting anions (e) and HA (f) with different concentrations on MTX removal efficiency by BMMA-H_2O_2. (g) The removal efficiency of BMMA-H_2O_2 for MTX in the actual lake water. (h) Regeneration of BMMA-H_2O_2 in five reused cycles.

Table 1 The removal performance of various materials for MTX

Material	MTX concentration (mg L^{-1})	Dosage (g L^{-1})	Performance	Mechanism	Ref.
BMMA-H_2O_2	20	0.2	1 min, 97.7%; 30 min, 99.7%	Adsorption	This work
Mn NPs	20	0.2	90 min, 97.4%	Adsorption	37
rGO/Fe NPs	30	0.2	180 min, 99.8%	Pre-adsorption and fenton-like oxidation	38
rGO@Fe NPs	20	0.8	5 min, 95%; 20 min, 98.5%	Adsorption	39

H_2O and BMMA-H_2O_2 samples are significantly improved (inset of Fig. 3a). BMMA-H_2O has a higher rate of MTX removal than BMMA in the same amount of time. Both samples achieve the adsorption equilibrium in 2 h, and their respective removal efficiencies are 99.58% and 99.59%. In contrast, BMMA-H_2O_2 shows excellent adsorption performance for MTX and achieves ultrafast MTX removal. Within one minute, the removal efficiency of MTX reaches 97.66%, and it reaches the adsorption equilibrium after 30 min with a removal efficiency of up to 99.72%. Surprisingly, BMMA-H_2O_2 has a much quicker rate of adsorption and higher adsorption performance than other materials (Table 1), which may be because pore filling and functional group interaction are involved in the adsorption of MTX by moxa ash. The substantial SSA and evenly dispersed pores encourage the development of active adsorption sites,[35] meanwhile the ball milling process is conducive to exposing more oxygen-containing functional groups in moxa ash that are able to bond more to MTX molecules.[36] In addition, BMMA-H_2O_2 can also be used to adsorb dyes (malachite green and methylene blue) in wastewater with very high removal efficiency (Fig. S2†), making it a universal adsorption material for environmental remediation.

Fig. 3b shows the effect of dosage of moxa ash adsorbents on MTX removal efficiency before and after modification. With an increase in dosage, four adsorbents are more effective in removing MTX and virtually all follow the same pattern. However, for MA, the removal efficiency of MTX improves more slowly, reaching a maximum of 98.57% at 1 g L^{-1} dosing levels. At the same dosage level, BMMA and BMMA-H_2O remove MTX substantially more quickly than MA does, which may be more active adsorption sites on the material surface. For BMMA-H_2O_2, it can remove 99.12% of MTX at a dose of 0.2 g L^{-1}, and the removal efficiency rises marginally and achieves saturation at 99.72% when the dose is raised to 0.5 g L^{-1}.

The effectiveness of MTX removal by moxa ash is affected by the pH of the solution both before and after the modification, as shown in Fig. 3c. When the pH is between 2 and 12, they exhibit a similar pattern. MA, BMMA, BMMA-H_2O, and BMMA-H_2O_2, all maintain their greatest removal efficiencies and stay essentially steady when the pH levels fall between 4 and 10. When MTX and additional H^+ ions compete for adsorption sites at pH = 2, the surface functional groups of moxa ash are protonated under acidic circumstances, leading to a considerable drop in removal efficiency.[39] Besides, a certain degree of decline in removal efficiency occurs at pH = 12. This is because high concentration of OH^- in a strongly alkaline environment can increasingly promote the combination of H^+ in MTX with the OH^- in solution, ultimately leading to the loss of more ions bound to moxa ash.

Fig. 3d shows how the initial MTX concentration affects the adsorption capacity of moxa ash. The four samples exhibit comparable trends, with the adsorption capacity for MTX increasing with the initial concentration. Obviously, the three ball-milled samples display higher adsorption capacity than that of MA. At a starting MTX concentration of 200 mg L^{-1}, BMMA-H_2O_2 has a larger adsorption capacity than MA (253.87 mg g^{-1}), measuring 301.80 mg g^{-1}. MTX may be virtually completely removed by BMMA-H_2O_2 with a starting concentration of less than 50 mg L^{-1}. The relative active sites on the surface of moxa ash decrease as the MTX concentration rises, which causes the rate of growth in adsorption capacity to be slower.[40]

Fig. 3e illustrates that the adsorption capacity of BMMA-H_2O_2 decreases with increasing ionic strength. However, Cl^-, SO_4^{2-} and NO_3^- have no significant effect on their removal of MTX, and only CO_3^{2-} exhibits pronounced inhibition. Probably due to the hydrolysis of CO_3^{2-} can produce OH^- to increase the pH value of solution, which affects the adsorption capacity of MTX by BMMA-H_2O_2. HA is widely distributed in water and usually present in the range of 1–5 mg L^{-1} in ordinary surface water.[41] Obviously, it is clear from Fig. 3f that HA in this concentration range did not influence the adsorption performance of BMMA-H_2O_2. The results in Fig. 3g show that the rate of BMMA-H_2O_2 in adsorption of MTX in lake water was inhibited at the initial stage of adsorption by the interference of various ions and organic matter, but sufficient active sites still ensured its high removal efficiency as the adsorption process continued. Therefore, the above results demonstrate that BMMA-H_2O_2 has excellent anti-interference ability and show great potential in practical applications. In addition, regeneration of BMMA-H_2O_2 using NaOH was able to fully release the adsorbed MTX into the solution (Fig. 3i). High removal rate of MTX (98.31%) was maintained after five reused cycles, indicating that BMMA-H_2O_2 has excellent sustainable adsorption performance.

3.3 Adsorption kinetics

Analysis of the adsorption rate according to the pseudo-first-order model eqn (3) and the pseudo-second-order model eqn (4).

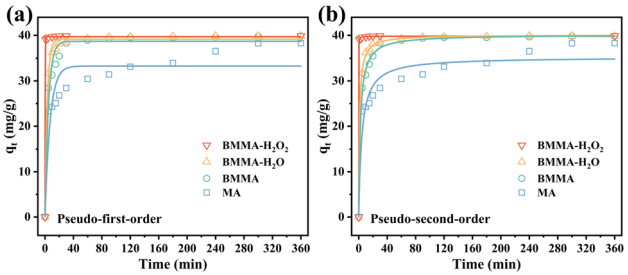

Fig. 4 Adsorption kinetics of MTX by MA, BMMA, BMMA-H_2O and BMMA-H_2O_2, (a) the pseudo-first-order model and (b) the pseudo-second-order model.

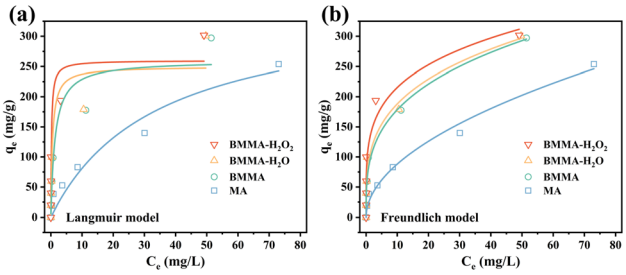

Fig. 5 Adsorption isotherms of MTX by MA, BMMA, BMMA-H_2O and BMMA-H_2O_2, (a) the Langmuir model and (b) the Freundlich model.

$$\ln(q_e - q_t) = \ln q_e - k_1 t \quad (3)$$

$$\frac{t}{q_t} = \frac{1}{k_2 q_e^2} + \frac{t}{q_e} \quad (4)$$

where q_e (mg g^{-1}) is the adsorption capacity at reaction equilibrium, q_t (mg g^{-1}) is the amount of MTX adsorbed on moxa ash at time t (min), k_1 and k_2 are the pseudo-first-order and pseudo-second-order rate constants, respectively.

The adsorption-related kinetic parameters of the model are provided in Table S2,† and the adsorption kinetic fitting curves are shown in Fig. 4. In comparison to the pseudo-first-order model (R^2 = 0.8426–0.9998), the pseudo-second-order model (R^2 = 0.9315–0.9999) provides the most accurate description of the MTX adsorption process, demonstrating that the rate of MTX adsorption by moxa ash is controlled by chemical mechanisms and may involve electron sharing or transfer between them.[42]

3.4 Adsorption isotherms

Isothermal sorption data are fitted using Langmuir eqn (5) and Freundlich eqn (6) models.

$$\frac{C_e}{Q_e} = \frac{C_e}{Q_m} + \frac{1}{Q_m K_L} \quad (5)$$

$$\ln Q_e = \frac{\ln C_e}{n} + \ln K_F \quad (6)$$

where C_e (mg L^{-1}) is the equilibrium concentration of MTX in solution and Q_e (mg g^{-1}) is the equilibrium adsorption amount. Q_m (mg g^{-1}) is the maximum adsorption capacity, K_L denotes the Langmuir model constant, K_F is the constant related to the adsorption capacity and intensity under the Freundlich model, and $1/n$ is the Freundlich constant.

Fig. 5 shows the adsorption isotherms fitting curves of MTX by MA, BMMA, BMMA-H_2O and BMMA-H_2O_2, and the parameters of the Langmuir and Freundlich isotherm models were also included in Table S3.† From the comparison of R^2, the adsorption process is more compatible with the Freundlich model, which demonstrates that MTX may create multilayer adsorption on moxa ash.[43] The statistics demonstrate that BMMA-H_2O_2 has the highest adsorption capacity since K_F value is often positively correlated with the adsorption capacity of adsorbent. The $1/n$ of BMMA-H_2O_2 is in the range of 0.1–0.5, indicating that the adsorption process includes multiple adsorption mechanisms and is easily carried out,[44] further confirming the ultrafast adsorption of MTX by BMMA-H_2O_2.

3.5 Probable mechanism of MTX removal

Moxa ash can increase its external specific surface area after ball milling and widen the internal pore space by chemical modification of H_2O_2. The enhanced adsorption capacity was positively correlated with the increase in external SSA and PV obtained by ball milling. It indicates that pore filling plays a role in the adsorption process. As shown in Fig. 6a, the XPS C 1s spectra of BMMA-H_2O_2 can be divided into four sub-peaks, C–C/C=C (284.8 eV), C–O (286.5 eV), C=O (288.0 eV) and O=C–O (289.9 eV). Upon adsorption of MTX, the decrease in the C–C/C=C ratio suggest that the graphite structure in moxa ash did participate in the π–π interaction process associated with the adsorption of MTX.[45] And the other three absorption peaks were blue-shifted to 286.9 eV, 288.5 eV, and 290.1 eV respectively, indicating that C–O, C=O and O=C–O on the moxa ash can act as electron donor and undergo π–π interaction with the benzene ring as electron acceptor on MTX.

The FTIR spectra (Fig. 6b) show that BMMA-H_2O_2 exhibit decrements in peak intensity and peak shifts of the functional groups after the adsorption of MTX. Thereinto, the peak corresponding to –OH bending vibration shifts from 3386 to 3406 cm^{-1} and the alkoxy C–O bending vibration shifts from 1046 to 1060 cm^{-1}. Apparently, the interaction between the oxygen-containing functional groups in MTX and BMMA-H_2O_2 result in the formation of hydrogen bond.[46] Additionally, the peak of the aromatic C=C/C=O bond skeleton vibration shifts from 1597 to 1618 cm^{-1}, demonstrating the existence of π–π interactions between MTX and moxa ash, which is consistent with the XPS analysis. Moxa ash is always negatively charged and therefore may adsorb positively charged N groups of MTX. Moreover, the pH value of solution and CO_3^{2-} concentration both affect the adsorption capacity of BMMA-H_2O_2, indicating that electrostatic attraction also contributes to the adsorption process. In summary, the adsorption mechanism of MTX by moxa ash is shown in Fig. 6c, which mainly involves pore filling, π–π interaction, hydrogen bond and electrostatic attraction.

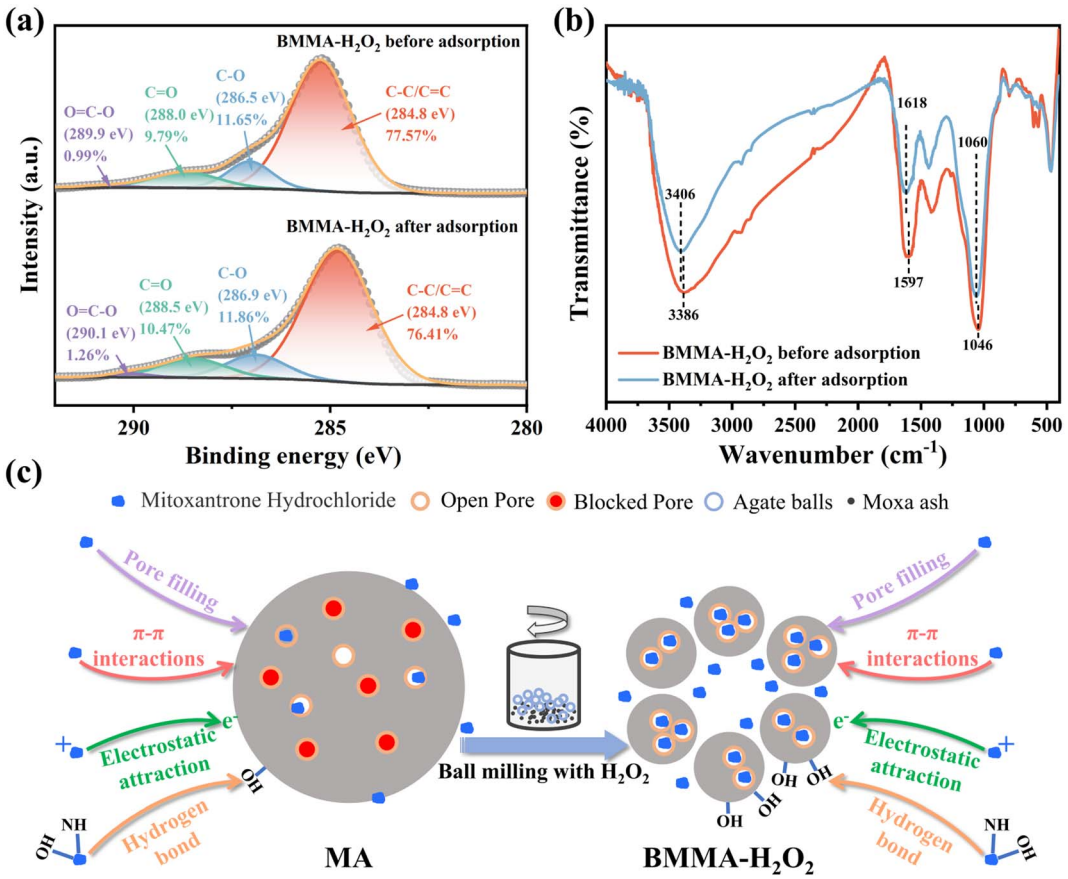

Fig. 6 The XPS C 1s (a) and FTIR (b) spectra of BMMA-H_2O_2 before and after MTX adsorption. (c) Comparison of possible adsorption mechanisms of MTX by MA and BMMA-H_2O_2.

4. Conclusions

In this study, moxa ash was modified under different ball milling environments, and the results showed that BMMA-H_2O_2 prepared by ball milling in hydrogen peroxide presents the best adsorption capacity to achieve ultrafast removal of MTX from water, which is more prominent than previously reported processes or materials for MTX removal. The powerful adsorption capacity was attributed to the increase of specific surface area and the number of functional groups during the modification process. BMMA-H_2O_2 not only possesses good resistance to interference and regeneration to ensure its application in real waters, but also serves as an excellent adsorbent for dye removal. It is worth noting that the green modification process of moxa ash will provide a reference for the management of antineoplastic drug pollution as well as an idea for converting more waste biomass into beneficial water treatment materials.

Author contributions

Wanqian Cai: investigation, methodology, data curation, and writing – original draft. Chongbiao Zhang, Yourong Wu, Wei Wang: conceptualization, methodology. Mei Lin: writing – reviewing and editing, supervision. Tengfei Lin: formal analysis. Cong Lin: validation. Min Gao: investigation. Chunlin Zhao: resources. Xiao Wu: supervision, investigation, writing – reviewing and editing.

Conflicts of interest

The authors declare that they have no conflict of interest.

Acknowledgements

This work was financially supported by the National Natural Science Foundation of China (No. 52072075, 52102126 and 12104093) and the Natural Science Foundation of Fujian Province (No. 2021J05122, 2021J05123, 2022J01087 and 2022J01552), and Qishan Scholar Financial Support from Fuzhou University (GXRC-20099).

References

1 A. P. P. da Rosa, R. P. Cavalcante, D. A. da Silva, L. D. M. da Silva, T. F. da Silva, F. Gozzi, E. McGlynn, A. Brady-Boyd, G. A. Casagrande, H. Wender, S. C. de Oliveira and A. M. Junior, *Sci. Total Environ.*, 2019, **651**, 2845–2856.
2 A. Yadav, E. R. Rene, M. K. Mandal and K. K. Dubey, *Chemosphere*, 2021, **263**, 128285.

3 M. S. Rehman, N. Rashid, M. Ashfaq, A. Saif, N. Ahmad and J. I. Han, *Chemosphere*, 2015, **138**, 1045–1055.
4 A. Osowski, A. Kasparek, Z. Wieczorek, R. Amarowicz and M. Szabelski, *Food Chem.*, 2017, **227**, 142–148.
5 C. Gómez-Canela, B. Campos, C. Barata and S. Lacorte, *Int. J. Environ. Sci. Technol.*, 2015, **12**, 633–640.
6 Z. Zhu, Z. Chen, X. Luo, W. Zhang and S. Meng, *Chem. Eng. J.*, 2020, **399**, 125650.
7 W. Chen, J. Mo, X. Du, Z. Zhang and W. Zhang, *Water Res.*, 2019, **151**, 243–251.
8 W. Zhang, W. Liang and Z. Zhang, *J. Membr. Sci.*, 2022, **663**, 120979.
9 Y. Xiang, Z. Xu, Y. Wei, Y. Zhou, X. Yang, Y. Yang, J. Yang, J. Zhang, L. Luo and Z. Zhou, *J. Environ. Manage.*, 2019, **237**, 128–138.
10 R. X. Guo, F. Z. Zheng and J. Q. Chen, *RSC Adv.*, 2015, **5**, 76772–76778.
11 D. Kanakaraju, B. D. Glass and M. Oelgemöller, *J. Environ. Manage.*, 2018, **219**, 189–207.
12 H. Wang, J. Xu, X. Liu and L. Sheng, *J. Clean. Prod.*, 2021, **283**, 124671.
13 C. Du, Z. Zhang, G. Yu, H. Wu, H. Chen, L. Zhou, Y. Zhang, Y. Su, S. Tan, L. Yang, J. Song and S. Wang, *Chemosphere*, 2021, **272**, 129501.
14 A. F. D. Silva, J. L. D. S. Duarte and L. Meili, *Sep. Purif. Technol.*, 2021, 264.
15 M. Du, Y. Zhang, Z. Wang, M. Lv, Q. Xu, Z. Chen, Q. Wen and A. Li, *Sep. Purif. Technol.*, 2022, **298**, 121585.
16 K. Wang, Y. Wang, S. Zhang, Y. Chen, R. Wang and S. Ho, *Environ. Sci. Ecotechnol.*, 2022, **10**, 100168.
17 D. M. Juela, *Sep. Purif. Technol.*, 2022, **284**, 120286.
18 M. E. Peñafiel, J. M. Matesanz, E. Vanegas, D. Bermejo, R. Mosteo and M. P. Ormad, *Sci. Total Environ.*, 2021, **750**, 141498.
19 Y. J. Dai, K. X. Zhang, X. B. Meng, J. J. Li, X. T. Guan, Q. Y. Sun, Y. Sun, W. S. Wang, M. Lin, M. Liu, S. S. Yang, Y. J. Chen, F. Gao, X. Zhang and Z. H. Liu, *Chemosphere*, 2019, **215**, 163–172.
20 Y. Zhang, L. Kang, H. Li, X. Huang, X. Liu, L. Guo and L. Huang, *Bioresour. Technol.*, 2019, **288**, 121516.
21 M. Ren, Y. Liu, X. Ni, Z. Kuang, X. Luo, Y. Zhang, H. Li and Y. Chen, *Integr. Med. Res.*, 2022, 100886.
22 Y. J. Xiang, Z. Y. Xu, Y. Y. Wei, Y. Y. Zhou, X. Yang, Y. Yang, J. Yang, J. C. Zhang, L. Luo and Z. Zhou, *J. Environ. Manage.*, 2019, **237**, 128–138.
23 M. Kumar, X. N. Xiong, Z. H. Wan, Y. Q. Sun, D. C. W. Tsang, J. Gupta, B. Gao, X. D. Cao, J. C. Tang and Y. S. Ok, *Bioresour. Technol.*, 2020, **312**, 123613.
24 J. Huang, A. R. Zimmerman, H. Chen and B. Gao, *Environ. Pollut.*, 2020, **258**, 113809.
25 Z. Huang, Y. Yi, N. Zhang, P. E. Tsang and Z. Fang, *Environ. Sci. Pollut. Res. Int.*, 2022, **29**, 33335–33344.
26 G. D. Qi, Z. F. Pan, X. Y. Zhang, X. D. Miao, W. Xiang and B. Gao, *Chem. Eng. J.*, 2022, **450**, 138027.
27 X. Zhang, X. Miao, W. Xiang, J. Zhang, C. Cao, H. Wang, X. Hu and B. Gao, *J. Hazard. Mater.*, 2021, **403**, 123540.
28 H. Lyu, S. Xia, J. Tang, Y. Zhang, B. Gao and B. Shen, *J. Hazard. Mater.*, 2020, **384**, 121357.
29 X. Zhu, Y. Liu, F. Qian, C. Zhou, S. Zhang and J. Chen, *Bioresour. Technol.*, 2014, **154**, 209–214.
30 H. Lyu, B. Gao, F. He, A. R. Zimmerman, C. Ding, H. Huang and J. Tang, *Environ. Pollut.*, 2018, **233**, 54–63.
31 B. Munkhbayar, M. J. Nine, J. Jeoun, M. Bat-Erdene, H. Chung and H. Jeong, *Powder Technol.*, 2013, **234**, 132–140.
32 L. Li, S. Liu and J. Liu, *J. Hazard. Mater.*, 2011, **192**, 683–690.
33 X. Wei, X. Wang, B. Gao, W. Zou and L. Dong, *ACS Omega*, 2020, **5**, 5748–5755.
34 W. Zhang, L. Yan, Q. Wang, X. Li, Y. Guo, W. Song and Y. Li, *J. Environ. Chem. Eng.*, 2021, **9**, 106870.
35 Q. Zhang, J. Wang, H. Lyu, Q. Zhao, L. Jiang and L. Liu, *Sci. Total Environ.*, 2019, **659**, 1537–1545.
36 Z. Zhuang, L. Wang and J. Tang, *J. Hazard. Mater.*, 2021, **406**, 124676.
37 F. He, W. Cai, J. Lin, B. Yu, G. Owens and Z. Chen, *J. Clean. Prod.*, 2021, **293**, 126207.
38 J. Wu, M. Lin, X. Weng, G. Owens and Z. Chen, *Chem. Eng. J.*, 2021, **408**, 127273.
39 J. Wu, Z. Lin, X. Weng, G. Owens and Z. Chen, *Chemosphere*, 2020, **246**, 125700.
40 F. Güzel, H. Sayğılı, G. Akkaya Sayğılı, F. Koyuncu and C. Yılmaz, *J. Clean. Prod.*, 2017, **144**, 260–265.
41 N. Li and H. K. Lee, *J. Chromatogr. A*, 2001, **921**, 255–263.
42 Y. Zhang, Y. Zheng, Y. Yang, J. Huang, A. R. Zimmerman, H. Chen, X. Hu and B. Gao, *Bioresour. Technol.*, 2021, **337**, 125432.
43 K. Feng, Z. Xu, B. Gao, X. Xu, L. Zhao, H. Qiu and X. Cao, *Environ. Pollut.*, 2021, **290**, 117992.
44 L. Yan, L. Kong, Z. Qu, L. Li and G. Shen, *ACS Sustain. Chem. Eng.*, 2015, **3**, 125–132.
45 Y. Ma, T. Lu, J. Tang, P. Li, O. Mašek, L. Yang, L. Wu, L. He, Y. Ding, F. Gao, X. Qi and Z. Zhang, *Sep. Purif. Technol.*, 2022, **297**, 121426.
46 N. Huang, P. Zhao, S. Ghosh and A. Fedyukhin, *Appl. Energy*, 2019, **240**, 882–892.